ChemComm



COMMUNICATION

View Article Online



Cite this: Chem. Commun., 2025, **61**, 14129

Received 21st April 2025, Accepted 7th August 2025

DOI: 10.1039/d5cc02180d

rsc.li/chemcomm

On metal-organic framework isomers, and the SF₆ sorption and fluorescence of an In and a Zr MOF with a tritopic linker†

Hao Li,^a Francoise M. Amombo Noa, (10 * ab Michelle Åhlén, (10 ° Zhejian Cao, (10 d Joakim Andréasson, Da Ocean Cheung Da and Lars Öhrström D*

The concept of framework isomers by network topology analysis is illustrated by a new rod-MOF isomer of In3+ and the tritopic linker 4,4',4"-(benzene-1,3,5-triyl-tris(oxy))tribenzoic acid (H₃bttb), CTH-41, with a unique 3- and 4-connected net different from 437-MOF. CTH-41 shows affinity for SF₆ with a Langmuir area of 1587 m² g⁻¹ while the new Zr⁴⁺ dot-MOF with the same linker [Zr₆(bttb)₄(O)₄(OH)₄] CTH-42, forms the 3-, 12-connected lij-net based on a different conformation of the flexible bttb linker.

The discovery and determination of molecular isomers were essential for the development of organic chemistry 200 years ago, and coordination chemistry some 80 years later. Polymorphism can be viewed as the solid state analogue, and was also discovered in the 1820's. Polymorphs appear when materials with identical composition pack differently in their crystals, yielding different space groups and unit cells.

This also occurs for metal-organic frameworks (MOFs), when identical organic and inorganic secondary building units, SBUs, form topologically distinct networks.^{2,3} The analysis of framework isomerism is as essential for reticular chemistry as it once was for molecular chemistry, and still poorly understood.

We use $[In_3(bttb)_2(OH)_3]$ CTH-41, and 437-MOF to illustrate the importance of MOF framework isomerism, the geometry of SBUs and topology, see Fig. 1. $[Zr_6(bttb)_4(O)_4(OH)_4]$ CTH-42 is not a framework isomer to the previous but will be discussed from another angle.

Zhou and co-authors2 define framework isomers as MOFs with different network structures. Framework isomers can also be structures with similar but distinguishable conformational frameworks arising from different anions and solvents.4 The factors that create framework isomerism are typically temperature, solvent or templating molecules, concentrations and pH.⁵ To optimize the synthesis of phase pure materials is a nontrivial task requiring extensive condition screening. 6-8

Three groups of framework isomers have been identified.² The first and second are interpenetration isomers and conformational framework isomers. The last one, orientation framework isomers, is rare. These isomers consist of SBUs which, taken as independent entities, are indistinguishable based on atomic makeup, connectivity, symmetry or other factors. They are generated by different orientations of the SBUs within the frameworks,² and can normally be distinguished by their all-nodes network topologies.9

Good examples are the PCN-16 and PCN-16' MOFs discussed in ref. 2 where the "single node" deconstruction reported results in the same nbo-net for both MOFs.2 However, following the "all nodes" approach we find that these two MOFs indeed can be described in more detail as the 3- and 4-connected fog and fof nets respectively, see SI.

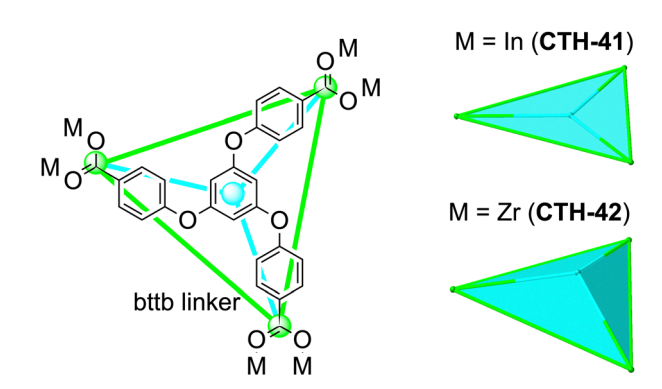


Fig. 1 The linker H₃bttb forming two MOF derivatives, [In₃(bttb)₂(OH)₃] CTH-41, and [Zr₆(bttb)₄(O)₄(OH)₄] CTH-42. The colored points and lines illustrate two limiting symmetric configurations of this flexible linker, the planar triangle as in CTH-41, (all in one plane) and the triangular pyramid (blue point above the plane) as in CTH-42.

^a Chemistry and Biochemistry, Dept. of Chemistry and Chemical Engineering, Chalmers University of Technology, SE-41296 Gothenburg, Sweden. E-mail: mystere@chalmers.se, ohrstrom@chalmers.se

^b School of Health Sciences, Catholic University of Central Africa, P.O. Box 1110,

^c Department of Materials Science and Engineering, Ångström Laboratory, Uppsala University, SE-751 03 Uppsala, Sweden

^d Department of Life Sciences, Chalmers University of Technology, SE-41296 Gothenburg, Sweden

[†] Dedicated to the memory of Professor Vratislav Langer 1949-2024.

Communication ChemComm

In this work, we employ the tritopic linker H₃bttb, which often adopts a triangular geometry in the solid state (Fig. 1), as we considered this an excellent candidate for the preparation of MOFs with framework isomers. The bttb linker has flexibility around its ether groups and can adopt several conformations, the two most symmetric being a planar triangle and a triangular pyramid, (Fig. 1), thus in theory producing various topologies.

The other reason for choosing H3bttb is that, based on analysis of the Cambridge Structural Database (CSD), 10 most MOFs synthesized with H₃bttb linker form 1D channels in their frameworks. 11-13 We find 1D channels preferable as the unidirectional nature of transport reduces cross-diffusion, which can improve separation performance, though it may make membrane fabrication more challenging. 14,15

Since bttb³⁻ is a O-terminated hard base ligand according to Hard and Soft Acid and Base (HSAB) theory, we chose to explore MOFs based on its strong interaction with hard Lewis acids, such as high valent Zr⁴⁺ and In³⁺ metal ions, for the purpose of building stable frameworks built from strong bonds.

Solvothermal synthesis in dimethylacetamide (dma) at 120 °C with In(NO₃)₃ gave the rod-MOF [In₃(bttb)₂(OH)₃], CTH-41 but with ZrCl₄ in dimethylformamide (dmf) and acetic acid at 120 °C [Zr₆(bttb)₄(O)₄(OH)₄] CTH-42 was formed. Both preparations gave crystals suitable for single crystal X-ray diffraction.‡

CTH-41 crystallises in a space group $P\bar{6}2c$ and has not only an identical formula to 437-MOF16 synthesised in dmf at 120 °C, but also the SBUs are identical, see Fig. 2.

Packing diagrams (Fig. S3), however, reveal these as two different structures, also reflected in their sorption properties where the derived pore size of 437-MOF is close to 30 Å whereas in CTH-41 it is nearer to 12 Å. We speculate that differences in hydrogen bonding, and in In³⁺ solvation, in dmf and dma might be one factor, see SI, Section S12.

Network analysis was used to distinguish between these framework isomers. We note that the network topology of 437-MOF has previously been described in different ways. 16,17 We apply here the most reductive method, the straight rod approach (STR) by adding mid-points between the metal ions and connecting the carbon atom of the COO bridge to the midpoint of the rod, (see SI, Section S3). 18,19



Fig. 2 Left: Crystal structure of [In₃(bttb)₂(OH)₃] CTH-41, and superposition of the organic SBUs and metal-SBUs of [In₃(bttb)₂(OH)₃] CTH-41, and $[ln_3(bttb)_2(OH)_3]$ **437-MOF**. Right: The nets in $[ln_3(bttb)_2(OH)_3]$ **CTH-41**, and [In₃(bttb)₂(OH)₃] **437-MOF** using the STR approach. The largest rings in the CTH-41 net is 8 whereas in tfz it is 10 nodes.

This approach now clearly distinguishes the two isomers: **437-MOF** forms the binodal $(3-c)_2(4-c)_3$ **tfz**-net (3-and 4-connected)based on triangles and squares whereas CTH-41 forms a new trinodal $(3-c)(3-c)(4-c)_3$ net with vertex symbol $(6^3)(8^3)(6^2.8^4)_3$, based on triangles and a see-saw, see Fig. 2. It is obvious that the tfz-net allows for larger channels, also indicated by the vertex symbols (SI, Section S3), with the largest rings in the CTH-41 net being 8-membered, but 10-membered in tfz.

The two MOFs CTH-41 and 437-MOF are orientational framework isomers,16 as the structures of the SBUs are near identical (Fig. 2) but they differ in their relative orientations. Specifically, for one linker in CTH-41 the relative SBU orientation is changed by 180° (Fig. S5) compared to 437-MOF.

Turning to [Zr₆(bttb)₄(O)₄(OH)₄] CTH-42, a classical dot-MOF,²⁰ the question is now what frameworks can be formed from the flexible tritopic bttb linker and the ubiquitous 12-connected $\{Zr_6(CO_2)_{12}(O)_4(OH)_4\}$ metal-SBU.²¹ The Zr_6 SBU normally forms of a cuboctahedron, a polyhedron with eight triangular and six square faces, that we now shall combine with the triangular SBU of the bttb.

In their survey of reticular chemistry motifs based on the geometry of the SBUs, Kalmutzki et al. show the rarity of combing 12-c nodes with triangular SBUs, citing the only examples as the skynet for the cuboctahedron, none for the icosahedron, the aea-net for the hexagonal antiprism, and ttt for the truncated tetrahedron.²²

A survey of the networks of more than 900 known MOFs based on the Zr₆ coordination entity reveals a striking lack of tritopic linkers, around 3% (see SI, Section S4). In a discussion of 4,12-c Zr-MOFs with 1,3,5,7-tetra(carboxyphenyl) benzene, Nateghi et al. noted that they could not obtain a MOF with a corresponding tritopic linker.²³ The well-known MOF-808 on the other hand adopts a 3,6-c spn topology by incorporating six formate terminating ligands into the $\{Zr_6(CO_2)_{12}(O)_4(OH)_4\}$ core.

CTH-42 crystallises in a tetragonal space group I4/m and the Zr₆ cluster indeed forms a cuboctahedron SBU just as in UiO-66.

The structure is shown in Fig. 3 together with the unusual llj-net that describes the structure. CTH-42 is a dot-MOF but still has pronounced 1D channels along the z-axis due to the conformation of the bttb linker, distinctively different from what is found in CTH-41 as illustrated in Fig. S6.

In contrast to the few 3,12-c Zr-MOFs in the CSD, the 4,12-c Zr-MOFs (>20%) are more common which we attribute to the match

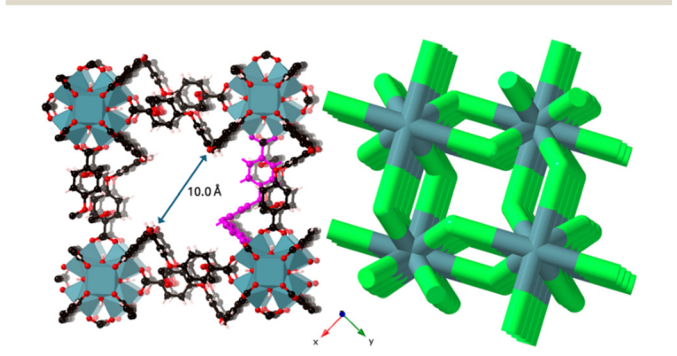


Fig. 3 $[Zr_6(bttb)_4(O)_4(OH)_4]$ CTH-42 with one bttb linker in pink, and the 3,12-c IIj net describing the structure. The narrowest diameter of the channels in z-direction is given

ChemComm

between the perfect cuboctahedron of the {Zr₆(CO₂)₁₂(O)₄(OH)₄} SBU and a square planar SBU in the ftw-net. In contrast there seems to be no known network that combines a perfect cuboctahedron with a perfect triangle.

The eight 3,12-c Zr-MOFs we have identified in the CSD have either the same llj-net as CTH-42, for example I-Rh,24 and ZrBTE, 25 or the sky-net as in MOF-1004.26

There is a good agreement of CTH-41 and CTH-42 calculated powder X-ray diffraction (PXRD) patterns with their respective assynthesised bulk materials, illustrated in Fig. S9 and S10. PXRD reveals that CTH-41 is stable in CH₂Cl₂, methanol, dmf, and dma, but shows peak broadening in water. CTH-42 loses crystallinity in water, methanol, and CH₂Cl₂, only retaining framework integrity in dmf, Fig. S10. While CTH-41 is stable for two years in room temperature CTH-42 transforms to other phases, thus suggesting an inherent instability of the framework in CTH-42.

Elemental analysis and thermogravimetry are consistent with solvent filled channels (SI, Sections S5 and S6) but also some linker deficiency in CTH-42, as sometimes observed with the Zr₆ SBU, see SI.²⁷ CTH-41 and CTH-42 show disintegration at temperatures above 400 °C and 500 °C respectively.

After synthesis, the MOFs were washed with dmf before solvent exchange at room temperature, first with anhydrous dmf 3 times and then anhydrous methanol 3 times and kept in methanol prior to supercritical CO₂ activation, see SI, Section S1.

The specific Brunauer-Emmett-Teller (BET) and Langmuir areas of CTH-41 estimated using the N2 adsorption isotherm were found to be 1378 and 1587 m² g⁻¹, respectively (Fig. S13(a) and Table S6), in good agreement with the value obtained from the single crystal data using the Mercury²⁸ pore analyser, 1701 m² g⁻¹. However, for CTH-42 the BET and Langmuir areas were estimated using CO₂, as N₂ adsorption kinetics on this framework was very slow, especially at low relative pressure. This gave areas of $305 \text{ m}^2 \text{ g}^{-1}$ and $383 \text{ m}^2 \text{ g}^{-1}$ respectively (Fig. S14(a) and Table S7), considerably lower than predicted by the pore analysis with Mercury, 2652 m² g⁻¹. Stability issues, as noted above, may be behind this discrepancy, as also the regeneration plot indicates gradual breakdown of CTH-42 between cycles (Fig. S17).

The pore size distributions were estimated using N₂ (CTH-41) and CO₂ (CTH-42) isotherms by the slit pore model and density functional theory, as seen in Fig. S13(b) and Fig. S14(b). CTH-41 showed one type of pore with estimated diameter of approximately 11.8 Å in good agreement with crystallographic data using Mercury, indicating 10.1–10.5 Å. Two distinct types of pores were detected for CTH-42 with estimated diameters of ~ 3.6 and ~ 5.3 Å, in reasonable agreement with the crystal structure showing larger channels of diameter 7.2 Å and a narrower more winding connection of cavities with diameters 4-5 Å. This agreement between experimentally derived pore size and the crystal structure further supports that partial structure collapse is behind the small surface area for CTH-42.

The N₂, CH₄, SF₆ and CO₂ adsorption isotherms of CTH-41 and CTH-42 at 20 °C are shown in Fig. 4, and we want to highlight the greenhouse gas SF₆. The SF₆ adsorption isotherm of CTH-41 shows a gradual increase at low pressures, indicating that the pore with approximate diameter of 11.8 Å, which is noticeably larger than the kinetic diameter of SF₆ (5.5 Å), is most likely too large

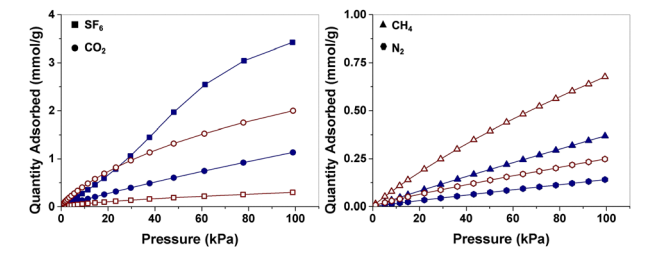


Fig. 4 N₂, CH₄, SF₆ and CO₂ adsorption isotherms of CTH-41 (blue, closed symbols) and CTH-42 (brown, open symbols) recorded at 20 °C.

for the enhanced SF₆ interaction of other MOFs discussed in our previous studies. 29,30 The total uptake, however, is reasonably good with more than 3.3 mmol g⁻¹ at 1 bar and the isosteric heat of sorption is 27.3 to 21.4 kJ mol^{-1} (0.05–2.70 mmol g^{-1} SF₆, Fig. S15). It is worth noting that the SF₆ isotherm of CTH-41 shows an S shape, and that the heat of SF₆ adsorption increases with the SF₆ uptake. This may suggest that with the internal surface of CTH-41 coated with initially adsorbed SF₆, the subsequent adsorbent-adsorbate interaction can be enhanced due to partial positive and negative charge separation at the newly formed internal surface from the large electronegativity difference between S and F.

For CTH-42, CO₂ uptake was the highest of the tested gases, indicating that CTH-42 has some selectivity towards CO2 over the other gases. The uptake at 1 bar (20 °C) reached a moderate 2.0 mmol g^{-1} with an isosteric heat of CO₂ sorption of around $21.6-24.2 \text{ kJ mol}^{-1}$ at up to 1.65 mmol g^{-1} loading (Fig. S16).

We also performed cyclic adsorption/desorption experiments on CTH-41 and CTH-42 using SF₆ and CO₂, respectively. CTH-41 shows complete regenerability over five SF₆ sorption cycles, but the less stable CTH-42 experienced a decrease of CO2 uptake of 3-4% per cycle (Fig. S17).

Due to the inherent fluorescence (Fig. S19), CTH-41 and CTH-42 were investigated as potential fluorescent sensors for organophosphorus pesticides. While established analysis protocols exist for these compounds, there is a need for off-grid solutions for rapid field tests for first responders, especially as these compounds also mimic, and are related to, chemical weapons such as sarin. 31,32

Here, paraoxon methyl (analogue to parathion-methyl) and a non-phosphate pesticide permethrin (Fig. 5) were investigated as they are difficult to monitor by visual inspection, indicated by the UV-Vis spectra of their dmf solutions (Fig. S21). The fluorescence of both MOFs can be quenched by the analyte species, which may have been facilitated by the 1D channels of the MOFs in terms of analyte diffusion and subsequent MOF-analyte interaction. As energy transfer reactions are excluded as the mechanism of quenching (little to zero spectral overlap) the most likely quenching mechanism is photoinduced electron transfer (PET). As CTH-41 is more stable in solvents than CTH-42, only this MOF was further investigated for fluorescence detection properties with the analytes paraoxon methyl and permethrin.

Quantitative data were obtained by dispersing CTH-41 in dmf and titrating with paraoxon methyl or permethrin, recording the fluorescence intensities (Fig. 5). Stern-Volmer analysis allowed us to determine the limit of detection (LOD) and limit of quantification (LOQ), which are 6.37 µM and 8.44 µM for Communication ChemComm

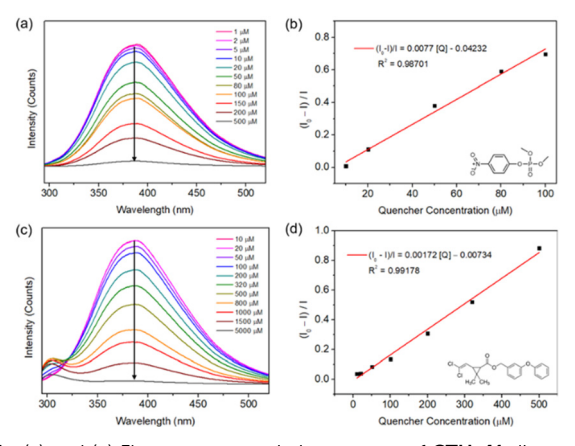


Fig. 5 (a) and (c) Fluorescence emission spectra of CTH-41 dispersed in dmf titrated with paraoxon methyl or permethrin; (b) and (d) Stern-Volmer fitting of the fluorescence intensities. Excitation for emission readout at 280 nm. For data on CTH-42 see SI.

paraoxon methyl, and 8.16 µM respectively 17.46 µM for permethrin (SI, Section S11).

This is similar to what was reported for a Cd-bttb MOF with parathion-methyl: LOD of 12 μM and LOQ of 39 μM , 12 demonstrating the capability of CTH-41 to detect organophosphates and insecticides at a trace level.

In conclusion we have shown the importance of orientation framework isomers by example of [In₃(bttb)₂(OH)₃] CTH-41, and 437-MOF and how they can be differentiated by network topology analysis. We also noted the high SF₆ capacity of CTH-41 and the unusual network topology of CTH-42, [Zr₆(bttb)₄(O)₄(OH)₄], and showed the possible quantification of the pesticides paraoxon methyl, and permethrin. Finally, we have explained the puzzling absence of 3,12-c Zr-MOFs by the network topology mismatch between a perfect cuboctahedron and a perfect triangle SBU. We also note further studies are warranted for CTH-42. These results show the continued relevance of network topology analysis in reticular chemistry and the possibilities framework isomerism offers for new MOF materials.

Conflicts of interest

There are no conflicts to declare.

Data availability

The data supporting this article have been included as part of the SI, as cif files, and an adsorption information (.aif) format file.

Supplementary information available: Synthesis and characterisation details. See DOI: https://doi.org/10.1039/d5cc02180d

CCDC 2444498 and 2444504 contain the supplementary crystallographic data for this paper. 34,35

Notes and references

‡ The reported MOFs were characterised by single crystal diffraction PXRD, TGA, SEM, and elemental analysis. Topologies were analysed with SYSTRE.³³ Gas sorption analyses were run on a Micromeritics ASAP2020.

- 1 J. Bernstein, Polymorphism in Molecular Crystals, Oxford University Press, New York, USA, 2002.
- 2 T. A. Makal, A. A. Yakovenko and H.-C. Zhou, J. Phys. Chem. Lett., 2011, 2, 1682-1689.
- 3 L. Öhrström and F. M. Amombo Noa, Metal-Organic Frameworks, American Chemical Society, 2020.
- 4 X.-Q. Lü, Y.-Q. Qiao, J.-R. He, M. Pan, B.-S. Kang and C.-Y. Su, Cryst. Growth Des., 2006, 6, 1910-1914.
- 5 N. Stock and S. Biswas, Chem. Rev., 2012, 112, 933-969.
- 6 B. Moulton and M. J. Zaworotko, Chem. Rev., 2001, 101, 1629-1658.
- 7 J.-P. Zhang, X.-C. Huang and X.-M. Chen, Chem. Soc. Rev., 2009, 38, 2385-2396
- 8 A. Karmakar, A. Paul and A. J. L. Pombeiro, CrystEngComm, 2017, 19, 4666-4695
- 9 C. Bonneau, M. O'Keeffe, D. M. Proserpio, V. A. Blatov, S. R. Batten, S. A. Bourne, M. S. Lah, J.-G. Eon, S. T. Hyde, S. B. Wiggin and L. Öhrström, Cryst. Growth Des., 2018, 18, 3411-3418.
- 10 C. R. Groom, I. J. Bruno, M. P. Lightfoot and S. C. Ward, Acta Crystallogr., Sect. B, 2016, 72, 171-179.
- 11 W. J. Phang, W. R. Lee, K. Yoo, B. Kim and C. S. Hong, Dalton Trans., 2013, 42, 7850-7853.
- 12 J. Zhang, W. Zhou, L. Zhai, X. Niu and T. Hu, CrystEngComm, 2020, 22, 1050-1056.
- 13 H.-J. Peng, G.-X. Hao, Z.-H. Chu, Y.-W. Lin, X.-M. Lin and Y.-P. Cai, RSC Adv., 2017, 7, 34104-34109.
- 14 Y. Liu, B. Zhang, D. Liu, P. Sheng and Z. Lai, J. Membr. Sci., 2017, 528, 46-54.
- 15 Y. Liu, J. Liu and J. Hu, BMC Chem. Eng., 2019, 1, 3.
- 16 M. Du, M. Chen, X.-G. Yang, J. Wen, X. Wang, S.-M. Fang and C.-S. Liu, J. Mater. Chem. A, 2014, 2, 9828-9834.
- 17 A. Schoedel, M. Li, D. Li, M. O'Keeffe and O. M. Yaghi, Chem. Rev., 2016, 116, 12466-12535.
- 18 L. S. Xie, E. V. Alexandrov, G. Skorupskii, D. M. Proserpio and M. Dincă, Chem. Sci., 2019, 10, 8558-8565.
- 19 P. Tshuma, B. C. E. Makhubela, L. Öhrström, S. A. Bourne, N. Chatterjee, I. N. Beas, J. Darkwa and G. Mehlana, RSC Adv., 2020, 10, 3593-3605.
- 20 F. M. Amombo Noa, M. Abrahamsson, E. Ahlberg, O. Cheung, C. R. Göb, C. J. McKenzie and L. Öhrström, Chem, 2021, 7, 2491-2512.
- 21 S. Yuan, L. Feng, K. Wang, J. Pang, M. Bosch, C. Lollar, Y. Sun, J. Qin, X. Yang, P. Zhang, Q. Wang, L. Zou, Y. Zhang, L. Zhang, Y. Fang, J. Li and H.-C. Zhou, Adv. Mater., 2018, 30, 1704303.
- 22 M. J. Kalmutzki, N. Hanikel and O. M. Yaghi, Sci. Adv., 2018, 4.
- 23 B. Nateghi, K. V. Domasevitch, R. Bulánek, C. Janiak and I. Boldog, Inorg. Chem., 2019, 58, 12786-12797.
- 24 T. Sawano, Z. Lin, D. Boures, B. An, C. Wang and W. Lin, J. Am. Chem. Soc., 2016, 138, 9783-9786.
- S. Won, S. Jeong, D. Kim, J. Seong, J. Lim, D. Moon, S. B. Baek and M. S. Lah, Chem. Mater., 2022, 34, 273-278.
- 26 S. Lee, H.-B. Bürgi, S. A. Alshmimri and O. M. Yaghi, J. Am. Chem. Soc., 2018, 140, 8958-8964.
- C. Koschnick, R. Stäglich, T. Scholz, M. W. Terban, A. von Mankowski, G. Savasci, F. Binder, A. Schökel, M. Etter, J. Nuss, R. Siegel, L. S. Germann, C. Ochsenfeld, R. E. Dinnebier, J. Senker and B. V. Lotsch, Nat. Commun., 2021, 12, 3099.
- 28 C. F. Macrae, I. J. Bruno, J. A. Chisholm, P. R. Edgington, P. McCabe, E. Pidcock, L. Rodriguez-Monge, R. Taylor, J. van de Streek and P. A. Wood, J. Appl. Crystallogr., 2008, 41, 466-470.
- 29 M. Åhlén, F. M. Amombo Noa, L. Öhrström, D. Hedbom, M. Strømme and O. Cheung, Microporous Mesoporous Mater., 2022, 343, 112161.
- 30 F. M. Amombo Noa, O. Cheung, M. Åhlén, E. Ahlberg, P. Nehla, G. Salazar-Alvarez, S. Ershadrad, B. Sanyal and L. Öhrström, Chem. Commun., 2023, 59, 2106-2109.
- 31 R. Burks and A. Winokur, in Encyclopedia of Forensic Sciences, ed. M. M. Houck, Elsevier, Oxford, 2023, pp. 263-277.
- 32 M. J. Kangas, R. Lukowicz, J. Atwater, A. Pliego, Y. Al-Shdifat, S. Havenridge, R. Burks, B. Garver, M. Mayer and A. E. Holmes, Anal. Chem., 2018, 90, 9990-9996.
- 33 O. Delgado-Friedrichs and M. O'Keeffe, Acta Crystallogr., Sect. A, 2003, 59, 351-360.
- 34 H. Li, F. M. Amombo Noa, M. Åhlén, Z. Cao, J. Andréasson, O. Cheung and L. Öhrström, CCDC 2444498: Experimental Crystal Structure Determination, 2025, DOI: 10.5517/ccdc.csd.cc2n1ps6.
- 35 H. Li, F. M. Amombo Noa, M. Åhlén, Z. Cao, J. Andréasson, O. Cheung and L. Öhrström, CCDC 2444504: Experimental Crystal Structure Determination, 2025, DOI: 10.5517/ccdc.csd.cc2n1pzd.